Microwave assisted synthesis of biocompatible europium-doped calcium hydroxyapatite and fluoroapatite luminescent nanospindles functionalized with Poly (acrylic acid)

Alberto Escudero,[1] Mauricio Calvo,[1] Sara Rivera,[2] Jesús M. de la Fuente,[2] and Manuel Ocaña.[1]*

[1]Instituto de Ciencia de Materiales de Sevilla (CSIC-Universidad de Sevilla), C/ Américo Vespucio 49, E- 41092 Seville, Spain.

[2]Instituto de Nanociencia de Aragón, Universidad de Zaragoza, C/ Mariano Esquillor s/n, E-50018, Zaragoza, Spain.

aescudero@icmse.csic.es

KEYWORDS: Hydroxyapatite, Fluoroapatite, Nanospindles, Nanophosphors Functionalization, PAA.

ABSTRACT: Europium-doped calcium hydroxyapatite and fluoroapatite nanophosphors functionalized with poly acryl acid (PAA) have been synthesized through a one-pot microwave-

assisted hydrothermal method from aqueous basic solutions containing calcium nitrate, sodium phosphate monobasic, PAA, as well as sodium fluoride in the case of the fluoroapatite particles. In both cases a spindle-like morphology was obtained, resulting from an aggregation process of smaller subunits which also gave rise to high specific surface area. The size of the nanospindles was 191 (32) x 40 (5) nm for calcium hydroxyapatite and 152 (24) x 38 (6) nm for calcium fluoroapatite. The luminescent nanoparticles showed the typical red luminescence of Eu^{3+}, which was more efficient for the fluoroapatite particles than for the hydroxyapatite. This is attributed to the presence of OH^- quenchers in the latter. The nanophosphors showed negligible toxicity for Vero cells. Both PAA-functionalized nanophosphors showed a very high (up to at least one week) colloidal stability in MES at pH 6.5, which is a commonly-used buffer for physiological pH. All these features make both kinds of apatite-based nanoparticles promising tools for biomedical applications, such as luminescent biolabels and tracking devices in drug delivery systems.

TEXT

Nanoparticles are attracting interest in nanomedicine not only due to their potential medical applications,[1] ranging from optical biolabels and contrast agents for magnetic resonance imaging[2-5] to carriers for drug and gene delivery for disease therapy.[6-8] All these applications require uniform nanoparticles with controlled size, shape, composition, surface chemistry, and other physicochemical properties.[9] For example, a large surface area is required for drug delivery.[10] It is also known that the particle geometry plays an important role in cell-material interactions, affecting cellular uptake and cell functioning.[11]

Several luminescent nanomaterials[12] such as quantum dots,[13] nanostructures functionalized with organic dyes[14] and rare earth (RE) based phosphors have been suggested to be used as optical biolabels for imaging of tissues or intracellular structures, as sensors to detect biological molecules or as tracking devices. RE-based nanophosphors exhibit important advantages compared with the other available luminescent materials due to their lower toxicity, photostability, high thermal and chemical stability, high luminescence quantum yield, and sharp emission bands.[15] These nanophosphors usually consist of a host matrix such as fluorides,[16] phosphates,[17, 18] and vanadates,[19] doped with luminescent lanthanide cations. Among phosphates hosts, calcium hydroxyapatite is of special interest due to their high biocompatibility and good biodegradability.[20] This is caused by the fact that calcium phosphate is the inorganic mineral of human bone and teeth.[21] Calcium hydroxyapatite nanoparticles have been synthesized by different methods, based on precipitation,[22] sol-gel,[23] combustion,[24] emulsions,[25] hydrothermal,[26] and microwave assisted processes.[27, 28] Anisotropic calcium hydroxyapatite particles with a rod-like shape are by far the most common morphology reported in the literature, but other morphologies have also been described. For example, spherical particles of 250 nm and 26 nm have been obtained in presence of porphyrin[29] or from cyclohexane/water microemulsions,[30] respectively. Micrometric hollow spheres composed of rods have also been synthesized in water/N,N-dimethylformamide medium with tartrate additives,[31] and porous hollow microspheres have been synthesized though a DNA-templated hydrothermal method.[32]

It is also well-known that dispersions of calcium phosphate nanoparticles tend to agglomerate and sediment,[33] hindering any possible biomedical application. A further functionalization process is thus required in order to achieve colloidal stability. This process also provides anchors for adding functional ligands such as antibodies, peptides, proteins and some

anticancer drugs,[34] and can also be used to enhance the fluorescence intensity of the nanophosphors.[35] Functionalization of luminescent lanthanide-doped calcium hydroxyapatite nanoparticles with additives such as DNA[36] and 2-aminoethylphosphonic acid (AEP)[37, 38] have been reported. Poly(ethyleneimine) (PEI)-functionalized calcium hydroxyapatite nanoparticles have been suggested as transfection gene silencing systems,[39] whereas the functionalization of calcium phosphate nanoparticles with cell-specific antibodies leds to cell-specific targeting systems.[40] It has also been reported that europium-doped calcium hydroxyapatite ellipsoidal nanoparticles functionalized with AEP and folic acid exhibit a low cytotoxicity and can be internalized by ZR751 breast cancer cells.[41] Poly (acrylic acid) (PAA) is one of the polymeric ligands which is used for the biofunctionalization of nanoparticles, because of its negligible toxicity[42] and its hydrophilic character,[43] which make it feasible for a further functionalization with molecules of biomedical interest. The synthesis of hydroxyapatite nanocrystals in the presence of poly (acrylic acid) has been reported in the literature,[44, 45] although these procedures resulted in polydisperse, heterogeneous and aggregated particles.

In addition to calcium hydroxyapatite, calcium fluoroapatite shows also a good biocompatibility, at least as implant material.[46] It has more chemical and structural stability than hydroxyapatite[47] and it is expected to be a more efficient host material for luminescent applications due to the absence of OH^- that constitute possible quenching centers for the luminescence.[48] Calcium fluoroapatite white light emitting phosphors codoped with Ce^{3+} and Mn^{2+} have been reported.[49] However, no studies about the biological applications of calcium fluoroapatite nanophosphors can be found in the literature.

We report in this paper a novel and fast microwave-assisted method which is suitable for the one-pot synthesis of uniform and highly monodisperse Eu^{3+}-doped calcium hydroxyapatite

and Eu^{3+}-doped calcium fluoroapatite nanoparticles with a novel spindle-type morphology, and their functionalization with PAA. We show that this additive acts as morphology-directing agent and provides a high colloidal stability for the nanophosphors in biological buffer media (MES, pH 6.5). We also report for the first time a comparative study of the luminescence efficiency and cell toxicity of calcium hydroxyapatite and calcium fluoroapatite nanophosphors. The obtained results indicate that both kinds of nanophosphors may have potential biomedical applications, such as biolabels for *in vitro* assays.

Experimental section

Synthesis of the nanoparticles

Europium-doped calcium hydroxyapatite nanoparticles (sample EuHAp) were synthesized though a microwave–assisted method, as follows: an aqueous solution with the stoichiometric amount of sodium phosphate monobasic (NaH_2PO_4, Sigma, >99%) was added over an aqueous solution containing calcium nitrate tetrahydrate ($Ca(NO_3)_2 \cdot 4\ H_2O$, J.T. Baker 99.0 %), europium (III) nitrate pentahydrate ($Eu(NO_3)_3 \cdot 5\ H_2O$, Sigma, 99.9%), and poly (acrylic acid) (PAA, Sigma, Mw1800). The Eu/Eu+Ca molar ratio was 2 %. The final calcium, phosphate and PAA concentrations were 0.06 mol dm^{-3}, 0.036 mol dm^{-3} and 2 mg cm^{-3}, respectively, and the pH was adjusted to 11 by using aqueous ammonia. The milky solution produced after mixing was heated in a Sineo MDS-8 microwave oven at 180 ºC for one hour with a heating rate of 14 $ºC \cdot min^{-1}$. In order to get information on the mechanism of particles formation, some experiments were carried out under the same conditions but using shorter aging time (10 and 20 minutes) or higher PAA concentrations (20 $mg \cdot cm^{-3}$). Europium-doped calcium fluoroapatite nanoparticles (sample EuFAp) were synthesized following the same methodology but adding ten times the stoichiometric amount of sodium fluoride (NaF, Sigma, >99%) to the sodium phosphate

monobasic solution. For comparative proposes, both europium-doped calcium hydroxyapatite and calcium fluoroapatite nanoparticles were also synthesized in the same way but without using PAA as additive. In all cases, the resulting dispersions were cooled down to room temperature, centrifuged to remove the supernatants and washed twice with ethanol and once with double distilled water. Most of the nanoparticles were dispersed in water but some portions were dried at room temperature in order to carry out further characterization.

Characterization

The particle shape was examined by transmission electron microscopy (TEM, Philips 200CM). Particle size distributions were obtained by counting about one hundred particles from the TEM micrographs and by dynamic light scattering (DLS, Malvern Zetasizer Nano-ZS90) using nanoparticle suspensions in water (0.5 g cm^{-3}) at pH 7. The specific surface area of the luminescent nanoparticles was measured by N_2 adsorption using the BET isotherm in a Micromeritics' TriStar II Surface Area and Porosity System device. The chemical composition of the nanoparticles was studied by energy dispersive X-ray analysis in a Philips DX4 attached to the microscope. Calcium and europium contents were assessed by induced coupled plasma atomic emission spectroscopy (ICP-AES) in an ICP Horiba Jobin Yvon Ultima 2 spectrometer. Unless otherwise indicated, infrared spectra (FTIR) of the nanophosphors diluted in KBr pellets were recorded in a Jasco FT/IR-6200 Fourier transform spectrometer. In some cases the FTIR spectra were also obtained for the nanophosphors deposited on silicon wafers in order to avoid the interference of H_2O molecules existing in the KBr pellets. Thermogravimetric analyses (TGA) were performed in air at a heating rate of $10°C \cdot min^{-1}$, using a Q600 TA Instrument.

X-ray diffraction (XRD) studies were carried out using a Panalytical, X´Pert Pro diffractometer equipped with an X-Celerator detector. The crystallite size for several crystallographic directions was determined by using the Scherrer formula. A value of 0.9 for the K shape factor was employed. Zeta potential measurements of nanoparticle suspensions in water (0.5 $mg \cdot cm^{-3}$) at pH 7 were carried out in a Malvern Zetasizer Nano-ZS90 apparatus. The colloidal stability of the nanoparticle suspensions in 50 mM MES solutions (2-(N-Morpholino) ethanesulfonic acid, Sigma, 99%) at pH 6.5 was monitored by analyzing the evolution with aging time of both their UV-visible absorbance spectrum and the hydrodynamic particle diameter measured by DLS. For these analyses the nanoparticle concentration was set to 0.5 $mg \cdot cm^{-3}$.

Excitation and emission spectra of aqueous dispersions of the europium-doped nanoparticles in water suspensions (0.5 $mg \cdot cm^{-3}$) were recorded in a Horiba Jobin-Yvon Fluorolog FL3-11 spectrofluorometer operating in the front face mode. The photoluminescence quantum yield (QY), defined as the ratio between photons emitted and absorbed by the suspensions, was determined by an absolute method using an excitation wavelength of 393 nm. The used set up consisted of an integrating sphere (Labsphere) with its inner face coated with Spectralon, attached to the spectrofluorometer.[50] A non-fluorescent sample consisting of undoped calcium hydroxyapatite and calcium fluoroapatite nanoparticles having morphological characteristics similar to those of the analyzed europium-doped samples were used to mimic the scattering properties of the latter. Spectral correction curves for sphere and emission detector were provided by Horiba Jobin-Yvon. The photographs showing the luminescence of the nanophosphors in water dispersions with the same nanoparticle concentration were taken under illumination with ultraviolet radiation (λ= 254 nm), filtered from an Hg discharge lamp.

Biocompatibility studies of both europium-doped calcium hydroxyapatite and calcium fluoroapatite nanophosphors functionalized with PAA were undertaken by evaluating the cell viability of Vero (monkey kidney epithelial cells) by the MTT colorimetric assay.[51] Vero cells were cultured in Dulbecco's Modified Eagle's Medium (DMEM), supplemented with 10 % fetal bovine serum (FBS), 5 % glutamine and 5 % penicillin/streptomycin. Cell cultures were incubated at 37 ºC and equilibrated in 4 % CO_2 and air. For the cytotoxicity assay 5000 cells were seeded in each well of 96-well plates and grown for 24 hours. After 24 hours, the medium was replaced with fresh medium containing the different types of nanoparticles in varying concentrations. After cultivation again for 24 hours, 20 µL of MTT dye solution (5 $mg \cdot cm^{-3}$ in PBS) was added to each well. After 4 hours of incubation at 37 °C and 5 % CO_2, the medium was removed, the cells were washed with fresh medium, and formazan crystals were dissolved in 100 µL of DMSO. The absorbance of each well was read on a microplate reader (Biotek ELX800) at 570 nm. The spectrophotometer was calibrated to zero absorbance using culture medium without cells. The relative cell viability (%) related to control wells containing cell culture medium without nanoparticles was calculated by [A]test/[A]control x100. Each measurement was repeated at least five times to obtain the mean values and the standard deviation.

Results and discussion

a) Synthesis and physicochemical characterization europium-doped calcium hydroxyapatite and fluoroapatite nanophosphors

The protocol herein reported for the synthesis of the EuHAp sample resulted in the nanoparticles shown in Figure 1A. As observed, they present a spindle-like morphology, which has not been ever reported for this system. The particles show mean dimensions of 191 (32) x 40 (5) nm (axial ratio of about 4.8). The novel morphology of the particles can be attributed to the strong effect of PAA during the synthesis process, since a very different morphology consisting of nanorods with a broad size distribution between 50 and 90 nm was obtained when no PAA was used in the synthesis process (Figure S1A). The mean hydrodynamic diameter of the EuHAp particles obtained by DLS was 120 nm, which is value between the mean dimensions of the nanospindles obtained from the TEM images. This is expected for non-spherical particles free of aggregation. The observation of Figure 1A also reveals a rough particle surface which suggests a high specific surface area. This was confirmed by BET analysis, which gave a value of 86.1 $m^2 \cdot g^{-1}$ for this magnitude. Similar surface areas have been reported for rare earth doped hydroxyapatite nanorods which have been suggested as good candidates for drug delivery systems.[28] The successful incorporation of europium into the nanospindles was evidenced from the EDX spectrum obtained for single particles, which displayed europium peaks, in addition to those of calcium, phosphorous and oxygen (Figure S2A). ICP-AEP measurements resulted in an Eu/Eu+Ca molar ratio of 1.95 %, which is in agreement with the nominal value (2.0 %), thus indicating the complete incorporation of europium into the apatite matrix.

The nanoparticles obtained in presence of fluoride anions (sample EuFAp) also showed a spindle-like morphology, as it is shown in Figure 2A. These particles were however slightly smaller, showing mean dimensions of 152 (24) x 38 (6) (axial ratio 4) (table1). PAA plays also a

key role in the final morphological characteristic of the precipitates, since the particles synthesized in absence of PAA consisted of hexagonal prisms with mean dimensions 68 (16) x 15 (5) nm (Figure S1B). In agreement, the mean hydrodynamic diameter of the EuFAp nanoparticles obtained by DLS (102 nm) was also smaller than that of the EuHAp sample, and indicated that they were free of aggregation. The EuFAp particles showed a BET surface area of 86.3$m^2 \cdot g^{-1}$ which is similar to the measured for the EuHAp particles. The EDX spectrum carried out on a single particle confirmed the incorporation of europium into the nanospindles (Figure S2B). ICP-AEP measurements also gave in this case a Eu/Eu+Ca molar ratio (2.11 %) similar to the nominal value (2.0 %).

The FTIR spectra of both EuHAp and EuFAp samples are shown in Figure 3. The spectra contained the typical signals of calcium apatite,[52] including the bending vibrations of the phosphate groups around 600 cm^{-1} and their asymmetric stretching vibrations around 1050 cm^{-1}. The spectrum corresponding to the EuHAp sample showed a peak at 3560 cm^{-1} which did not appear on the spectrum of the EuFAp particles. This peak can be attributed to the OH^- ions, suggesting the formation of the hydroxyapatite phase.[53] In addition, a broad band centered at 3250 cm^{-1} and a weaker signal at around 1650 cm^{-1} were observed in both cases. They correspond to the O–H vibration and the H–O–H bending mode of absorbed water, respectively. The presence of PAA on the surface of the nanoparticles was also detected in the FTIR spectra of both PAA-functionalized samples. Signals corresponding to the vibrations of the CH_2 groups of the PAA were observed at 1454 cm^{-1} (scissor vibration) and around 2950 cm^{-1} (symmetric and asymmetric stretching vibrations, see the figure inset for magnification). In addition, the bands around 1415 and 1575 cm^{-1} can be ascribed to the symmetric and antisymmetric stretching

frequencies of the carboxylate ion (COO^-), respectively. Considering that the carbonyl stretching (C=O) vibration appears at 1717 cm^{-1} for the pure PAA, the shift towards lower frequencies observed in our case indicates that most of the carboxylate functional groups of the polymer are fully ionized,[54] and therefore, that the PAA molecules are bond to the nanoparticle surface though the carboxylate groups. It should be noted that calcium apatite particles usually absorb carbonate ions giving rise to low intensity bands appearing around 1400 cm^{-1} in the IR spectrum.[26] Indeed, signals at 1415 and 1459 cm^{-1} from CO_3^{2-} groups can be detected in the FTIR spectra of the samples synthesized in absence of PAA (Figure S3). The signals are however less intense than those observed for the PAA-functionalized samples (Figure 3). This finding along with the signal at 1575 cm^{-1} as well as the bands around 2950 cm^{-1}, which are absent in the spectra of the unfunctionalized samples, confirm unambiguously the presence of PAA on the surface of the PAA-functionalized particles. It must be mentioned that the relative intensity of the signals corresponding to PAA is lower in the EuFAp sample. This suggests that EuHAp particles are able to absorb more PAA onto their surface than the EuFAp particles.

An estimation of the amount of PAA on the surface of both EuHAp and EuFAp nanoparticles was obtained from TG analyses (Figure 4). Data corresponding to the samples synthesized in absence of PAA are also included in the figure for comparative reasons. As observed, both PAA-functionalized samples showed a weight loss in the 25 - 300 ºC range which can be ascribed to the release of absorbed water. This loss of water (6.6 % for the EuHAp particles and 5.6 % for the EuFAp sample) is higher than that found for the PAA-free samples (around 2 %). This can be attributed to the high surface area of the PAA-functionalized particles. An additional abrupt loss, which was not observed for the PAA-free particles, took place between 300 and 400 ºC in both

PAA-functionalized EuHAp and EuFAp samples. This should be caused by the decomposition of the PAA, which is known to occur in this range of temperatures.[55] Such a weight loss was lower for the EuFAp particles (5.4 %) than for the EuHAp sample (10.3 %), in good agreement with the FTIR observations. Finally, the slight weight losses observed at higher temperatures (2.3 % for the EuHAp sample in the 760 – 1000 ºC range and 2.5 % for the EuFAp sample at temperatures between 580 and 1000 ºC) should be connected with the dehydroxylation and defluorination of the apatite structures, respectively.

Further evidence of the PAA functionalization of the particles was obtained by comparing the Zeta potential of aqueous suspensions of both non-functionalized and PAA-functionalized particles. PAA-free hydroxyapatite particles showed Zeta potential of 1 mV at pH 7, whereas the value of this magnitude for the EuHAp nanoparticles was -24 mV at the same pH. A similar behavior was observed for the EuFAp sample. The Zeta potential of the PAA-functionalized nanoparticles was -32 mV, whereas that corresponding to the PAA-free particles was 1.5 mV. This charge reversal is consistent with the presence of PAA on the surface of both types of particles.

The XRD diagrams obtained for both the EuHAp and EuFAp particles (Figure 5) consist of peaks which match the standard pattern of $Ca_5(PO_4)_3(OH)$, calcium hydroxyapatite (PDF 01-084-1998), and $Ca_5(PO_4)_3F$, calcium fluoroapatite (PDF 00-015-0876), respectively. It must be noted that the signals corresponding to the fluoroapatite sample shifts slightly toward higher 2 theta angles (see for example the vertical guides in the figure) when compared with the

luminescent hydroxyapatite particles. This is consistent with the slightly higher unit cell volume of the fluoroapatite structure. No extra phases are observed in both diagrams.

The average crystal size (table 1) estimated by using the Scherrer formula from several XRD peaks (100, 002, 102 and 222) for both EuHAp and EuFAp particles was around 50 and 35 nm, respectively. These values are smaller than the dimensions of the nanoparticles, suggesting that the both kind of particles are polycrystalline. This was confirmed by HRTEM images, in which different crystalline domains could be observed within both a hydroxyapatite (Figure 1B) and fluoroapatite (Figure 2B) single particle. Such a polycrystalline character suggests that the nanospindles are formed through and aggregation process of small units.

In order to get stronger support for this mechanism of particle formation, the resulting hydroxyapatite precipitates obtained after different ageing times ranging from 10 minutes (which is the required time to reach a temperature of 180 ºC) to one hour were studied. TEM observations indicated that the initial milky solution produced after mixing the calcium and phosphate solutions consisted of a gel-like precipitate that accords to EDX data (not shown) contained calcium, phosphorous and oxygen, as well as low intensity signals corresponding to europium. Europium-doped calcium hydroxyapatite nanospindles were already formed just after reaching 180 ºC (10 minutes of heating), as it can be observed in Figure S4A. This indicates that the synthesis process is very fast, which is one of the main advantages of the microwave-assisted protocols.[56] The main dimensions of these nanospindles determined from the TEM image were 145 (23) x 31 (4) nm (axial ratio 4.7). These particles grew with increasing the aging time at 180 ºC and reached their final size of 191 (32) x 40 (5) nm after one hour (table 1). The average

crystallite size determined by using the Scherrer formula from the XRD data does not change appreciably with increasing the synthesis time (table 1). This strongly suggests that the nanospindles grow through an aggregation process of smaller subunits, which must be the reason of the rather high BET surface area measured for this sample. The role played by PAA in this aggregation process and therefore in determining the morphological features of the particles can be interpreted following the previous work of Jean and Ring on the synthesis of TiO_2 particles.[57] In principle, PAA molecules could be absorbed on the surface of the particles during the synthesis process and sterically stabilize them against further aggregation. However, when the nuclei are very small in size and thus they have a very large surface area per unit volume, the amount of added polymer may be insufficient to cover the complete surface of the particles. These processes involve aggregation until the surface area per unit volume is low enough that the added polymer provides stability. The amount of added polymer serves thus to control the particle size produced from aggregating species.[58] In order to confirm this suggestion, the synthesis was carried out under the same conditions but with a much higher amount of PAA (20 $mg \cdot cm^{-3}$). Figure S5A shows the so obtained europium-doped calcium hydroxyapatite particles, which resemble those synthesized with lower amount of PAA, but exhibit a much smaller size. In fact, their XRD pattern (Fig S5B) only shows some weak reflections corresponding to calcium hydroxyapatite with a large broadening, which indicates the smaller crystallite size of the particles.

Following the same methodology than in the europium-doped calcium hydroxyapatite nanoparticles, the europium-doped calcium fluoroapatite precipitates obtained after different aging times at 180 ºC were also analyzed. Europium-doped calcium fluoroapatite nanospindles

were found to be formed faster than the hydroxyapatite particles. Nanospindles with main dimensions of 142 (29) x 34 (7) nm (axial ratio 4.2) (table 1) resulted just after 10 minutes of microwave heating (Figure S4B), which were very similar to those formed after 20 minutes at 180 ºC (150 (18) x 36 (4) nm (axial ratio 4.2)) (table1). The faster kinetics of the process in this case should be connected with the lower solubility shown by calcium fluoroapatite.[59] Despite the scarce information obtained from these experiments on particle formation and considering that the crystallite size of the primary europium-doped fluoroapatite particles and their BET surface area were similar to those of the europium-doped calcium hydroxyapatite system, it can be stated that the fluoroapatite particles were also very likely formed thought an aggregation process of smaller units, in which PAA plays a key role in controlling the particle size.[58]

The colloidal stability in aqueous MES media at pH 6.5 of both PAA-functionalized EuHAp and EuFAp nanophosphors was analyzed by studying the evolution of theirs UV-visible spectra and the mean hydrodynamic diameter obtained by DLS with increasing the ageing time. The absorbance curve in both cases (Figure 6) did not change with increasing time, even after one week. This indicates the absence of sedimentation, which can be also visualized in the insets of Figure 6. In addition, no changes were observed in the mean hydrodynamic diameter of the nanoparticles for both EuHAp and EuFAp nanophosphors in this period of time (Figure 7), manifesting that no particle aggregation took place on aging. Therefore, it can be concluded that both apatite-based nanophosphors functionalized with PAA show a very high colloidal stability at physiological pH.

b) Optical properties of the europium-doped calcium hydroxyapatite and calcium fluoroapatite nanophosphors

Excitation spectra of both EuHAp and EuFAp nanophosphors (Figure 8A) were recorded by monitoring at wavelength of 618 nm, which corresponds to the main emission line expected for Eu (III) cations in the apatite matrix.[53] In both cases the spectra contained several bands in the region between 300 and 450 nm, the most intense one appearing at 393 nm, a wavelength close to the visible light domain. This band corresponds to the direct excitation of Eu^{3+} ions from the ground state $^7F_0$ to the $^5L_6$ excited level.[38] A secondary excitation peak assignable to the $^7F_0 \rightarrow {}^5D_2$ absorption appeared at 464 nm, within the visible range.[38]

Figure 8B shows the emission spectra of the suspensions of the EuHAp and EuFAp nanophosphors, recorded under a UV excitation of 393 nm. Both spectra were very similar and displayed the typical emissions corresponding to the $^5D_0$-^7F_J (J = 1, 2, 3, and 4) electronic transitions expected for the Eu^{3+} cation.[38, 53] It can be also observed that the relative intensity of the $^5D_0$-$^7F_2$ emission band in both europium-doped nanoparticles is higher than that associated with the $^5D_0$-$^7F_1$ transition, which is expected for Eu^{3+} cations located in crystallographic sites without an inversion center. This is compatible with Eu^{3+} cations replacing Ca^{2+} on the normal calcium sites of the apatite structure, in which the calcium sites show a local symmetry of C_3 and C_s.[60] The higher intensity of the emission in the 575-652 nm range give rise to a red light, as it is observed in the inset of the figure.

It also important to mention that the emission corresponding to the fluoroapatite sample exhibited higher intensity than the hydroxyapatite sample. This can be explained by the presence of OH^- groups in the latter sample, which are well-known to be effective quenchers of the europium luminescence.[48] Such a difference was confirmed by the higher luminescence quantum yield obtained for the europium-doped calcium fluoroapatite-based nanophosphors (6.1 %), when compared with that measured for the europium-doped calcium hydroxyapatite-based particles (2.1 %). To the best of our knowledge, the luminescent quantum yield has never been reported for europium-doped calcium hydroxyapatite and fluoroapatite nanophosphors and therefore a comparison of our efficiencies with other calcium apatite nanophosphors is not possible. Nevertheless, these rather low efficiencies when compared with other europium-based nanophosphors[56] can be ascribed to different factors. On one hand, crystalline defects arising from the polycrystalline character of the here reported nanospindles are known to play important roles in the decay mechanisms of the excited species and thus affect the quantum yield efficiency.[61, 62] On the other hand, the substitution of Ca^{2+} by Eu^{3+} is not isomorphic in the apatite structure, and other mechanisms such as Ca^{2+} vacancies, phosphate deprotonation and incorporation of either OH^- or of oxygen O^{2-} ions are required to keep the charge balance.[63] This may constitute potential quenching centers which can thus affect the quantum yield efficiency. Finally, the nanophosphors here reported are already functionalized with an organic polymer, which can also produce quenching effects and thus decrease the luminescent quantum yield efficiency.

c) Biocompatibility and cell viability of PAA-functionalized europium-doped calcium hydroxyapatite and calcium fluoroapatite nanophosphors

Biocompatibility studies of both kind of nanophosphors were undertaken by evaluating the cell viability of Vero cells by the MTT assay.[51] This assay relies on the mitochondrial activity of fibroblasts activity of fibroblasts and represents a parameter for their metabolic activity. The MTT (3-(4,5-dimethylthiazol-2-yl)-2,5-diphenyltetra-zolium bromide) assay is a simple non-radiactive colorimetric assay to measure cell cytotoxicity, proliferation, or viability. MTT is a yellow, water-soluble tetrazolium salt. Metabolically active cells are able to convert this dye into a water-insoluble dark-blue formazan by reductive cleavage of the tetrazolium ring. These formazan crystals can be dissolved in an organic solvent such as dimethylsulphoxide (DMSO) and quantified by measuring the absorbance of the solution at 550 nm, and the resultant value is related to the number of living cells. The metabolic activity and proliferation of fibroblasts was thus measured after 24 hours' culture, and showed negligible toxicity effects for both europium doped calcium hydroxyapatite and fluoroapatite nanophosphors (Figure 9), with viability percentages around 75-80 % for concentrations up 1.5 $mg \cdot cm^{-3}$. Such values are consistent with other previously reported in the literature,[41] thus confirming the low toxicity of this kind of apatite-based nanophosphors.

Conclusions

Calcium hydroxyapatite and calcium fluoroapatite-based nanophosphors doped with europium have been synthesized and functionalized with PAA following an one-pot microwave-

assisted hydrothermal protocol at 180 ºC which results in a novel morphology for these systems. In both cases, the obtained nanoparticles are polycrystalline and show a spindle-like shape with main dimensions of 191 (32) x 40 (5) nm for the calcium hydroxyapatite and of 152 (24) x 38 (6) nm for the calcium fluoroapatite-based nanophosphors. Both nanophosphors show the typical red luminescence corresponding to the Eu^{3+} cations, although the quantum efficiency of the fluoroapatite-based nanoparticles is higher than that of the analogous hydroxyapatite-based. This is explained by the quenching effect of OH^- on the europium luminescence. The presence of PAA on the surface of both kind of nanospindles results in very stable colloidal dispersions in MES at pH 6.5, as it is demonstrated by the of lack of sedimentation and particle aggregation on ageing up to at least one week. Both systems also show low cell toxicity. Because their luminescent properties, their low toxicity and the functionalization with PAA, which provides anchors for a further functionalization with molecules of biomedical interest, these nanophosphors are good candidates as potential tools for biomedical applications.

FIGURES

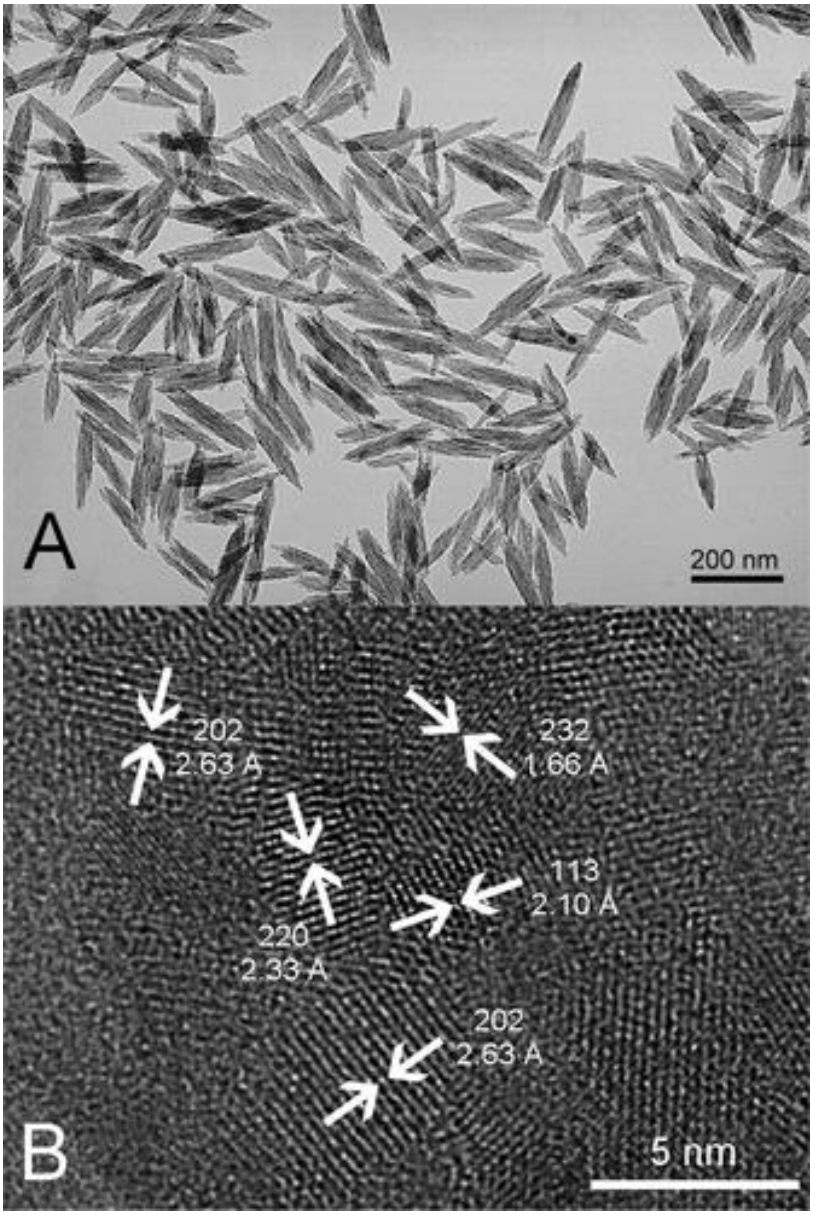

Figure 1. (A) TEM micrograph of the EuHAp nanophosphors functionalized with PAA. (B) HRTEM image of a single particle in which several planes compatible with the calcium hydroxyapatite structure, as well as the d spacings are shown.

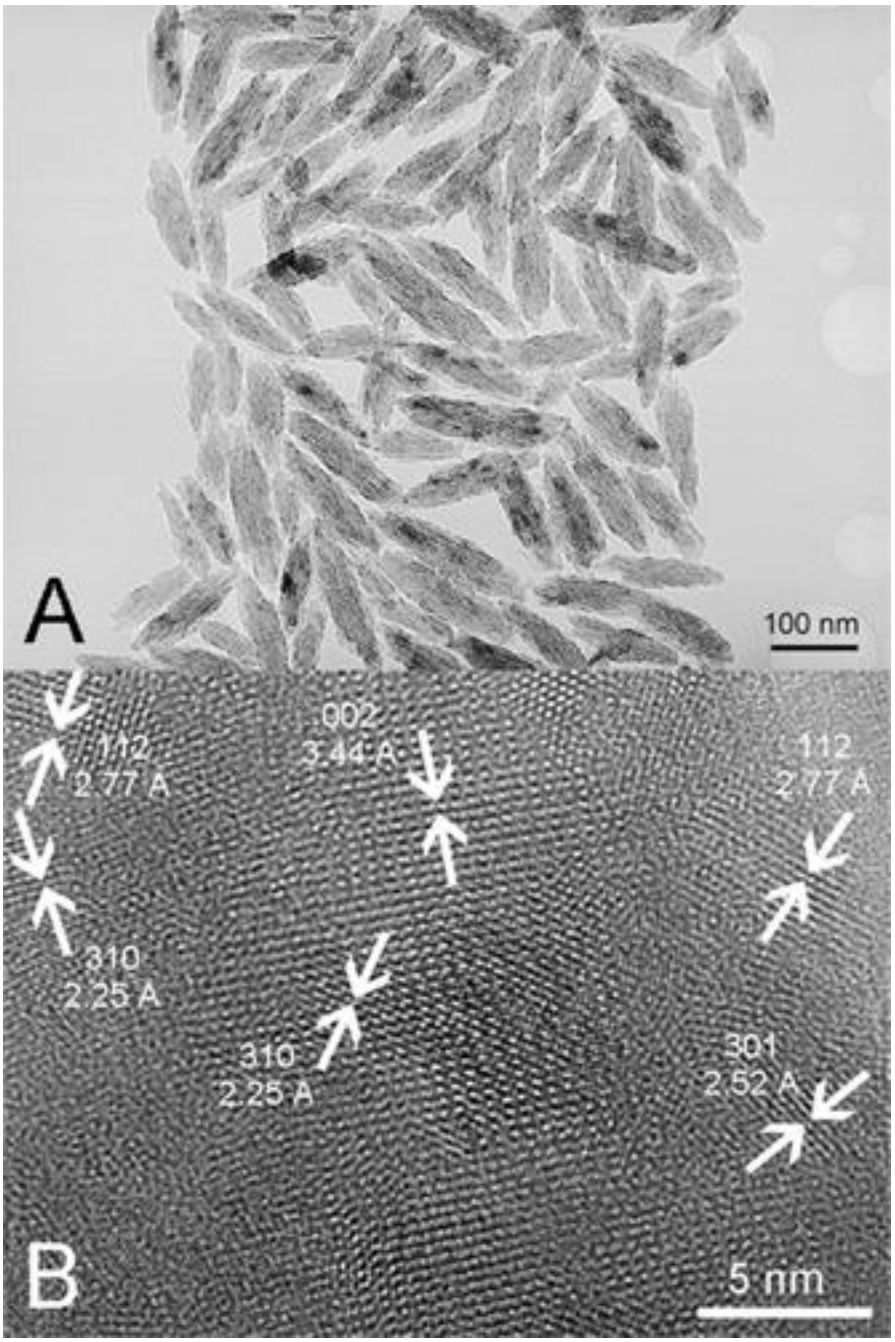

Figure 2. (A) TEM micrograph of the EuFAp nanophosphors functionalized with PAA. (B) HRTEM image of a single particle in which several planes compatible with the calcium fluoroapatite structure, as well as the d spacings are shown.

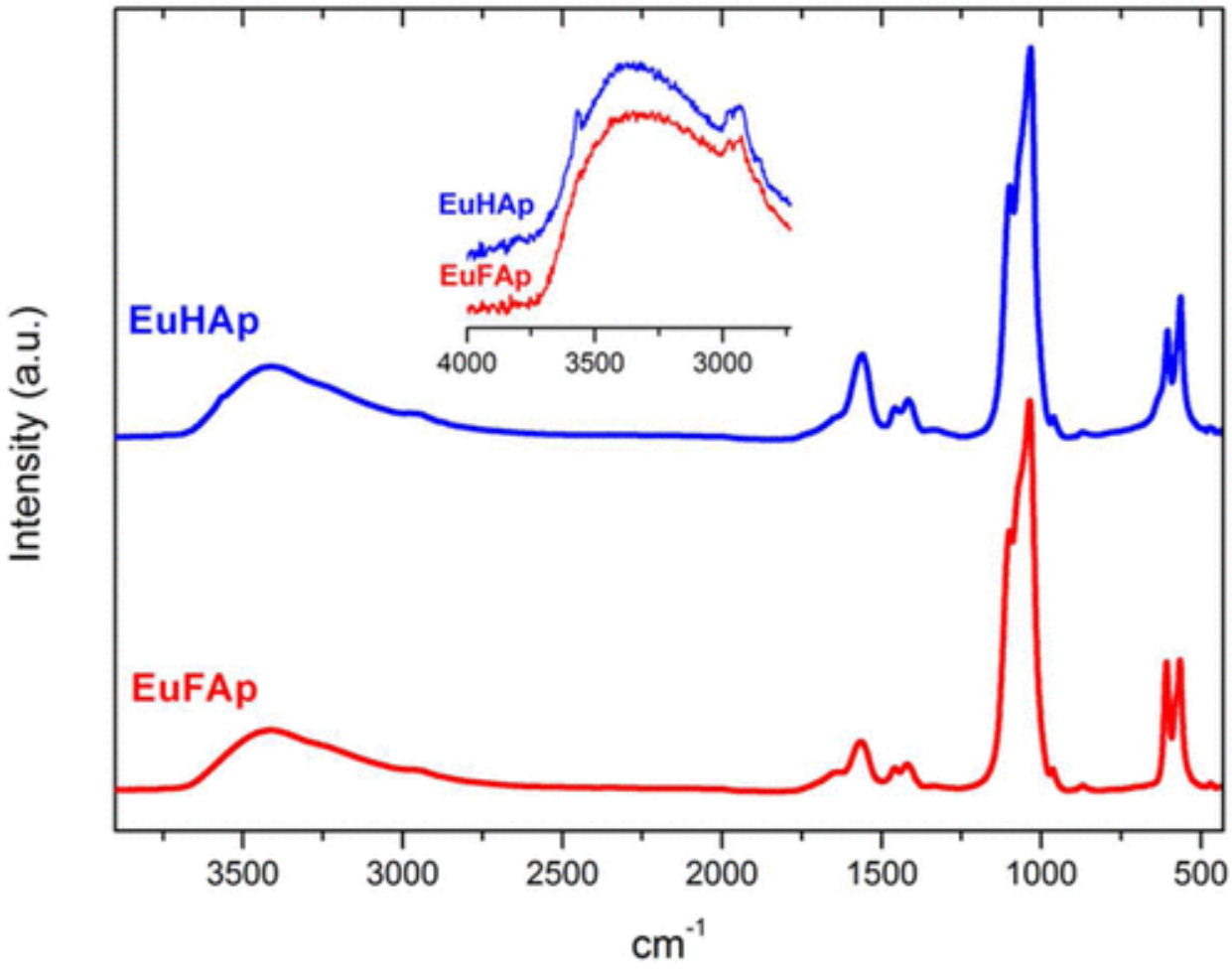

Figure 3. FTIR spectra of the EuHAp and EuFAp nanophosphors functionalized with PAA. The region from 4000 to 2600 cm^{-1} included in the upper part of the figure corresponds to the spectra of the same hydroxyapatite (EuHAp) and fluoroapatite (EuFAp) nanophosphors deposited on silicon wafers.

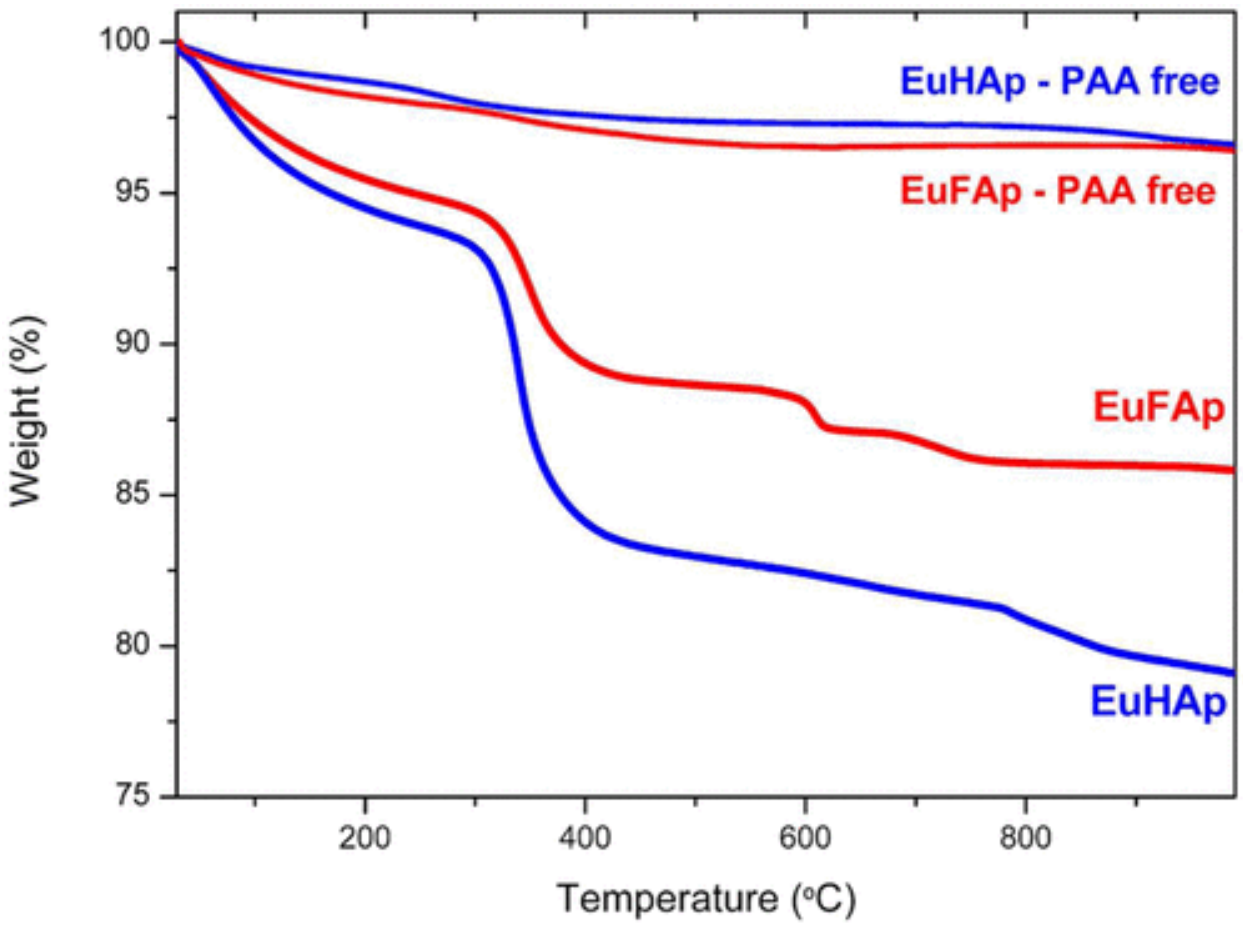

Figure 4. TGA analysis of the EuHAp and EuFAp nanophosphors functionalized with PAA. The curves corresponding to the samples synthesized in absence of PAA (EuHAp – PAA free and EuFAp – PAA free) are also included.

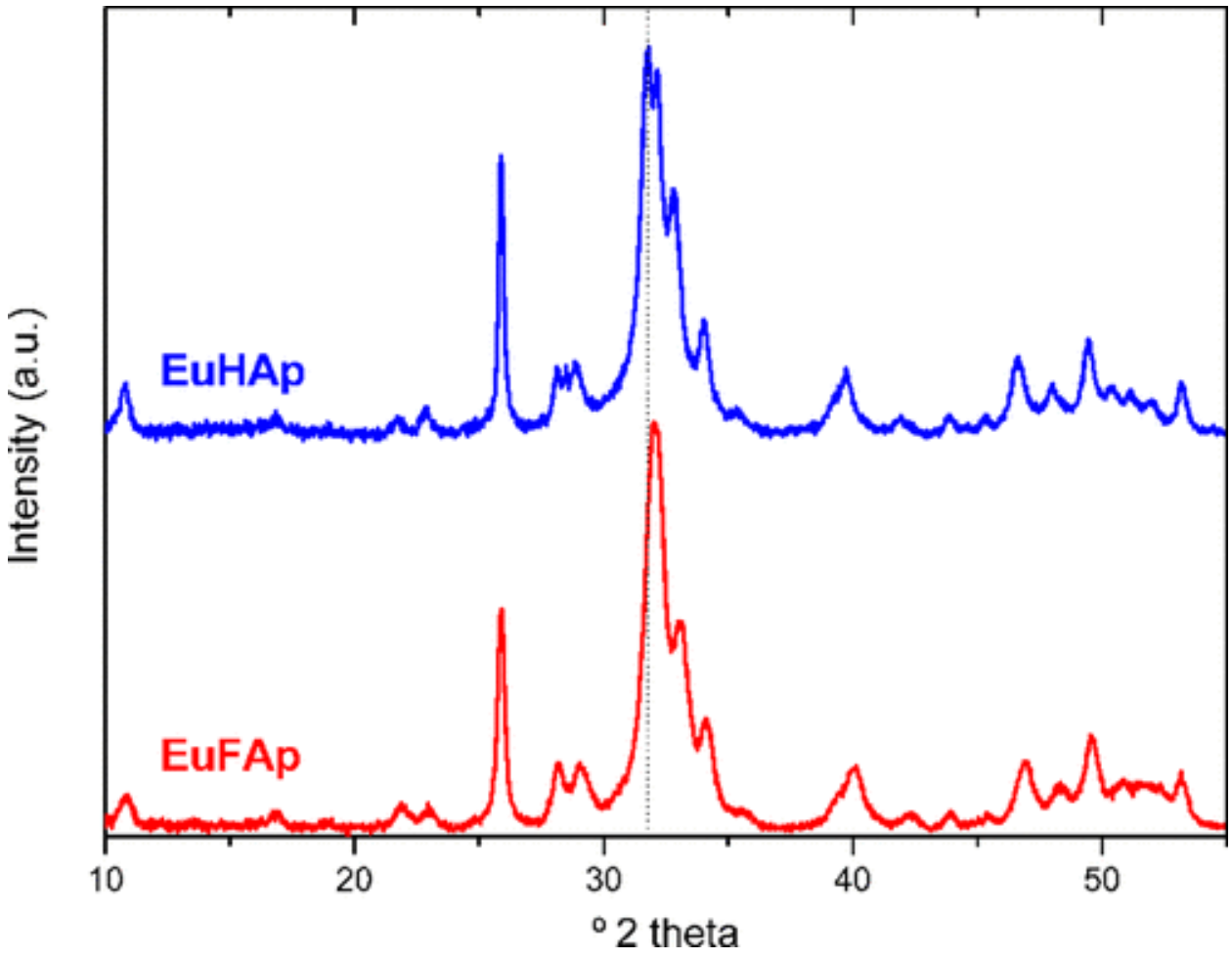

Figure 5. XRD diagrams of the EuHAp and EuFAp nanophosphors functionalized with PAA.

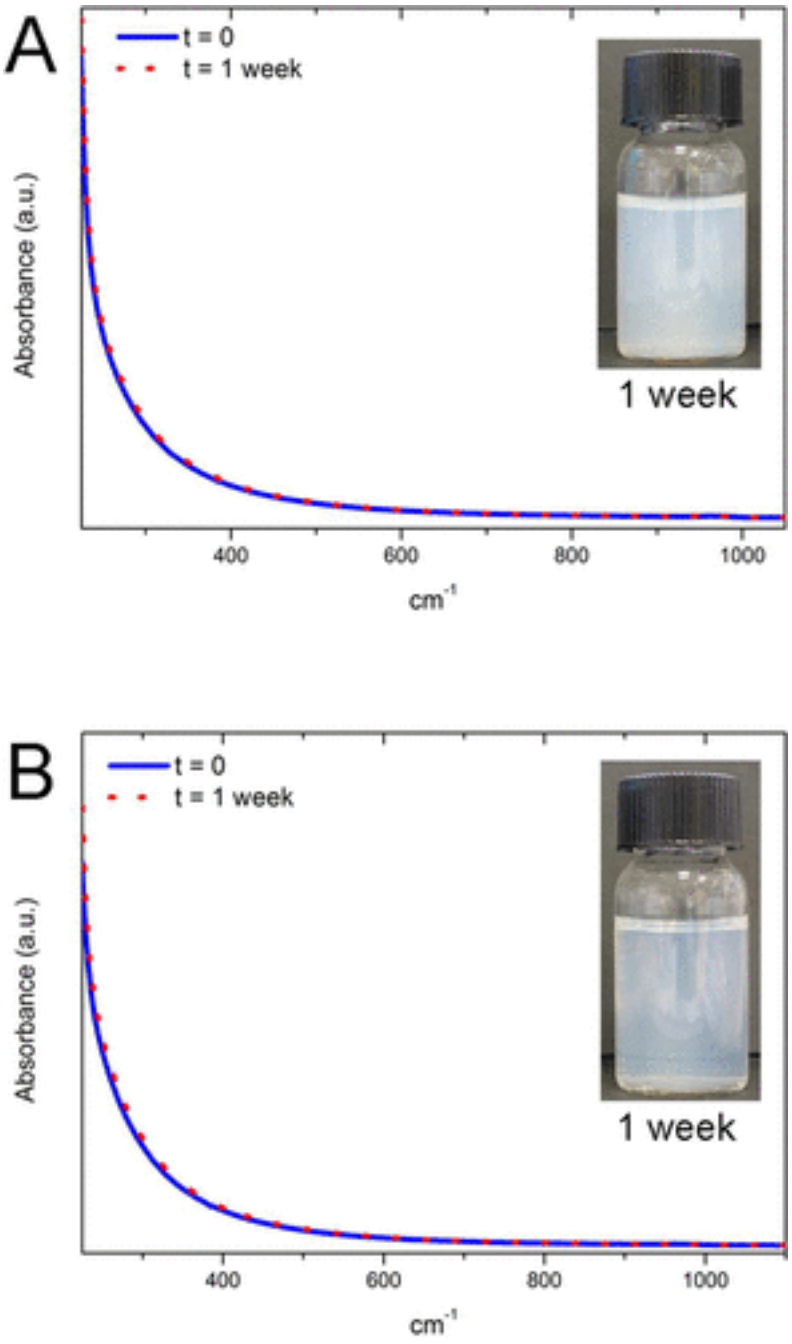

Figure 6. UV-visible spectra of the PAA-functionalized EuHAp (A) and EuFAp (B) suspensions in MES (50 mM) at pH 6.5 after different ageing times. Photos corresponding to the suspensions taken after one week are also included.

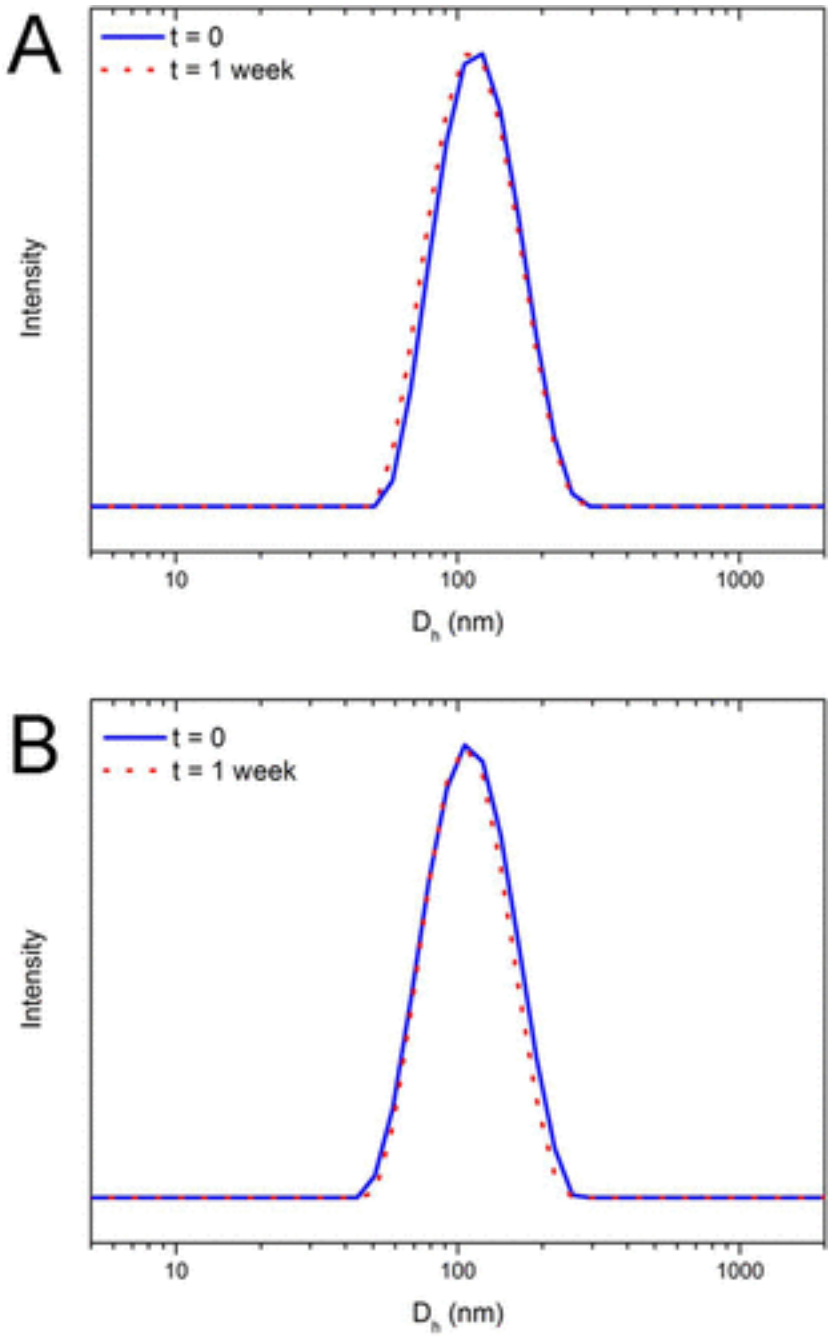

Figure 7. Size distributions determined by DLS for the PAA-functionalized EuHAp (A) and EuFAp (B) suspensions in MES 50 mM at pH 6.5 after different ageing times.

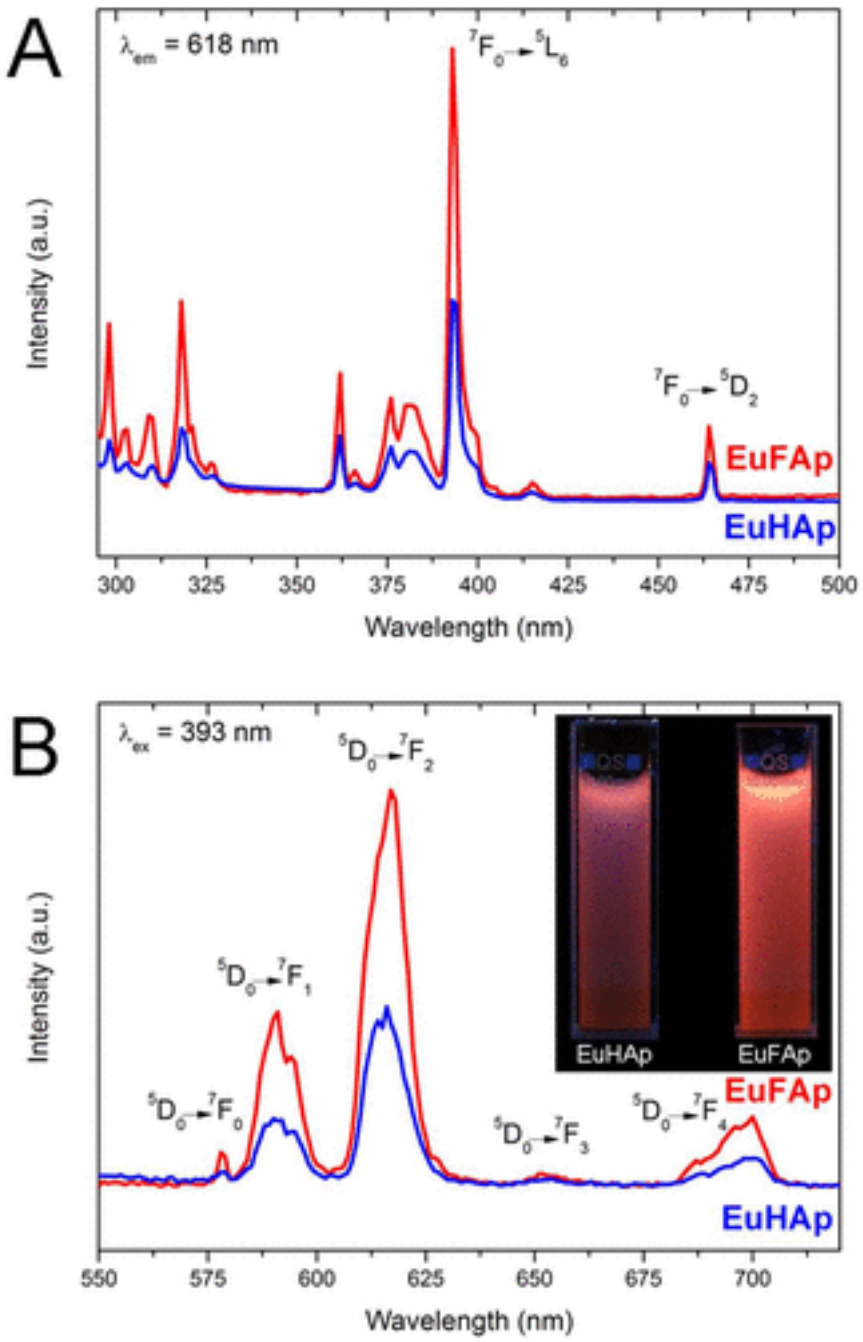

Figure 8. Excitation (monitored at 618 nm) (A) and emission (λ_{ex} 393 nm) (B) spectra of aqueous suspension of the PAA-functionalized EuHAp (blue) and EuFAp (red) nanophosphors. The image shows the luminescence of suspensions of EuHAp (left) and EuFAp (right) when irradiated with UV light.

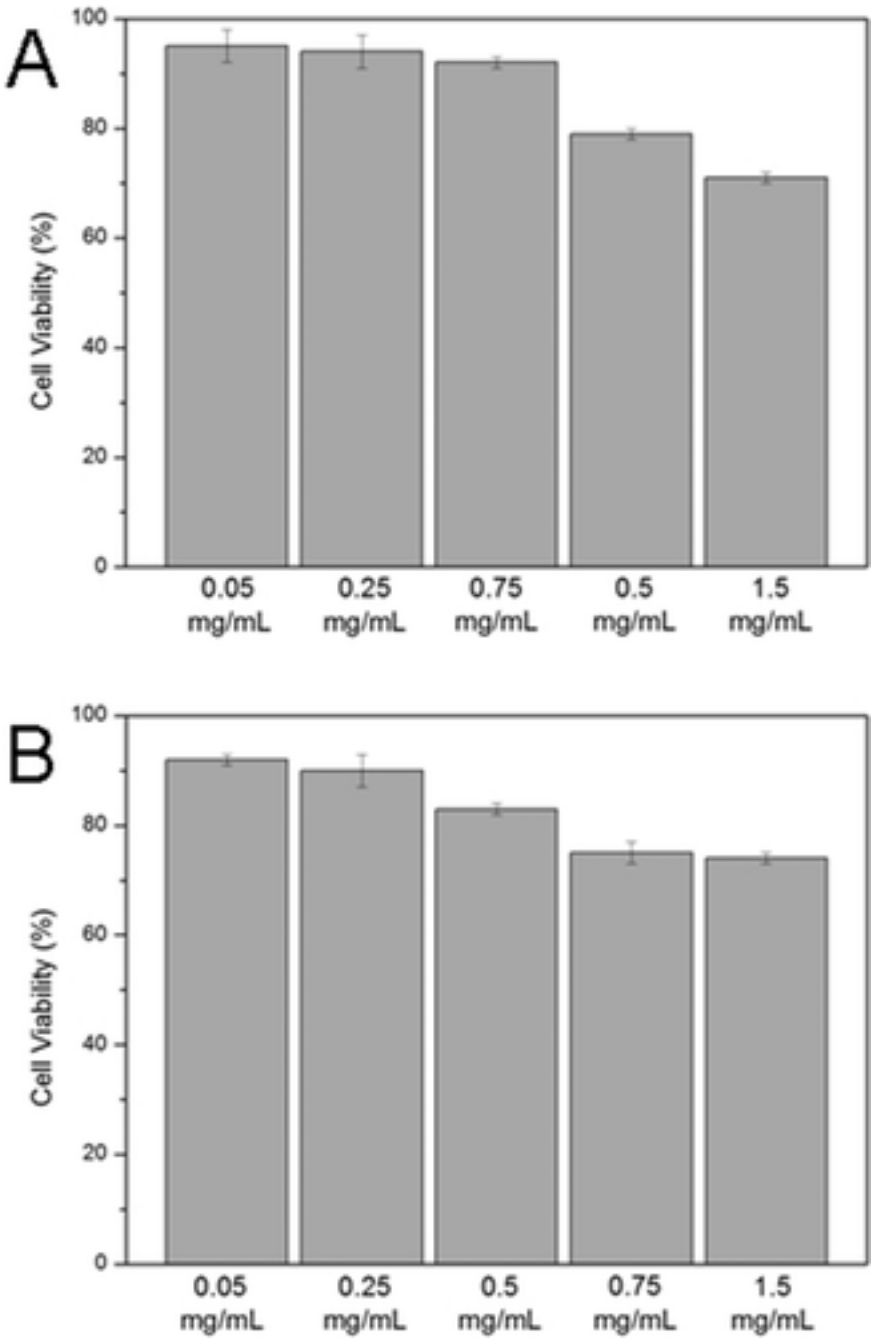

Figure 9. Viability assays performed with Vero cell line for different PAA-functionalized EuHAp (A) and EuFAp (B) nanophosphors at different nanoparticle concentrations. Results are represented as mean ± standard deviation

SCHEMES (Word Style “VC_Scheme_Title”). Chemical reactions and flow diagrams may be called schemes. Schemes may have brief titles describing their contents. The artwork for each scheme should immediately follow the scheme title. The title should follow the format “**Scheme 1.** Scheme Title”. All schemes must be mentioned in the text consecutively and numbered with Arabic numerals. Schemes may also have footnotes (use Word Style “FD_Scheme_Footnote”), inserted after the artwork.

CHARTS (Word Style “VB_Chart_Title”). Lists of structures may be called charts. Charts may have brief titles describing their contents. The title should follow the format “**Chart 1.** Chart Title”. Charts may also have footnotes (use Word Style “FC_Chart_Footnote”). To insert the chart into the template, be sure it is already sized appropriately and paste it immediately after the chart title.

TABLES.

Table 1. Mean particle dimensions and average size of the crystalline domains measured for the europium-doped calcium apatites synthesized at 180 ºC at increasing times. HAp = Calcium hydroxyapatite, FAp = Calcium fluoroapatite. All the samples are functionalized with PAA. Numbers in brackets indicate standard deviations.

	Synthesis time (minutes)	Main dimension (nm)	Short dimension (nm)	Axis ratio	Mean crystallite size (nm)
Eu-doped HAp-PAA	10	145 (23)	31 (4)	4.7	50.5
	20	173 (21)	37 (6)	4.7	47.3
EuHAp	60	191 (32)	40 (5)	4.8	45.7

Eu-doped FAp-PAA	10	142 (29)	34(7)	4.2	35.7
	20	150 (18)	36 (4)	4.2	35.5
EuFAp	60	152 (24)	38 (6)	4.0	35.5

AUTHOR INFORMATION

Corresponding Author

* Corresponding author. Phone +34 954489576, Fax +34 954460665 aescudero@icmse.csic.es

ACKNOWLEDGMENT

This work has been supported by the Junta de Andalucía (Grant FQM 6090), the Spanish Ministerio de Ciencia e Innovación (MAT2011-23593), and ERC-Starting Grant (NANOPUZZLE Project). Alberto Escudero thanks the Spanish National Research Council (CSIC) for a JAE-DOC contract. JMF thanks ARAID for financial support. Three anonymous reviewers are also acknowledged for their valuable comments to the manuscript and their constructive suggestions.

ASSOCIATED CONTENT

Supporting Information. TEM micrographs and FTIR spectra of the nanoparticles synthesized in absence of PAA, EDX spectra and TEM images and XRD diagrams of the nanospindles synthesized at different times. This material is available free of charge via the Internet at http://pubs.acs.org.

REFERENCES

1. Murthy, S. K. Nanoparticles in modern medicine: State of the art and future challenges. *Int. J. Nanomed.* **2007**, *2*, 129-141.

2. Liong, M.; Lu, J.; Kovochich, M.; Xia, T.; Ruehm, S. G.; Nel, A. E.; Tamanoi, F.; Zink, J. I. Multifunctional inorganic nanoparticles for imaging, targeting, and drug delivery. *ACS Nano* **2008**, *2*, 889-896.

3. Gao, X. H.; Cui, Y. Y.; Levenson, R. M.; Chung, L. W. K.; Nie, S. M. In vivo cancer targeting and imaging with semiconductor quantum dots. *Nat. Biotechnol.* **2004**, *22*, 969-976.

4. Fang, C.; Zhang, M. Q. Multifunctional magnetic nanoparticles for medical imaging applications. *J. Mater. Chem.* **2009**, *19*, 6258-6266.

5. Chatterjee, D. K.; Gnanasammandhan, M. K.; Zhang, Y. Small Upconverting Fluorescent Nanoparticles for Biomedical Applications. *Small* **2010**, *6*, 2781-2795.

6. Barreto, J. A.; O'Malley, W.; Kubeil, M.; Graham, B.; Stephan, H.; Spiccia, L. Nanomaterials: Applications in Cancer Imaging and Therapy. *Adv. Mater.* **2011**, *23*, H18-H40.

7. De Jaeghere, F.; Allemann, E.; Kubel, F.; Galli, B.; Cozens, R.; Doelker, E.; Gurny, R. Oral bioavailability of a poorly water soluble HIV-1 protease inhibitor incorporated into pH-sensitive particles: effect of the particle size and nutritional state. *J. Control. Release* **2000**, *68*, 291-298.

8. Schlachetzki, F.; Zhang, Y.; Boado, R. J.; Pardridge, W. M. Gene therapy of the brain - The trans-vascular approach. *Neurology* **2004**, *62*, 1275-1281.

9. Xia, Y. N. Nanomaterials at work in biomedical research. *Nat. Mater.* **2008**, *7*, 758-760.

10. De Jong, W. H.; Borm, P. J. A. Drug delivery and nanoparticles: Applications and hazards. *Int. J. Nanomed.* **2008**, *3*, 133-149.

11. Huang, X. L.; Teng, X.; Chen, D.; Tang, F. Q.; He, J. Q. The effect of the shape of mesoporous silica nanoparticles on cellular uptake and cell function. *Biomaterials* **2010**, *31*, 438-448.

12. Feldmann, C. Luminescent nanomaterials. *Nanoscale* **2011**, *3*, 1947-1948.

13. Gao, X. H.; Nie, S. M. Molecular profiling of single cells and tissue specimens with quantum dots. *Trends Biotechnol.* **2003**, *21*, 371-373.

14. Wang, F.; Tan, W. B.; Zhang, Y.; Fan, X. P.; Wang, M. Q. Luminescent nanomaterials for biological labelling. *Nanotechnology* **2006**, *17*, R1-R13.

15. Wang, G. F.; Peng, Q.; Li, Y. D. Lanthanide-Doped Nanocrystals: Synthesis, Optical-Magnetic Properties, and Applications. *Accounts Chem. Res.* **2011**, *44*, 322-332.

16. Núñez, N. O.; Ocaña, M. An ionic liquid based synthesis method for uniform luminescent lanthanide fluoride nanoparticles. *Nanotechnology* **2007**, *18*.

17. Núñez, N. O.; Liviano, S. R.; Ocaña, M. Citrate mediated synthesis of uniform monazite $LnPO_4$ (Ln = La, Ce) and Ln:$LaPO_4$ (Ln = Eu, Ce, Ce plus Tb) spheres and their photoluminescence. *J. Colloid Interface Sci.* **2010**, *349*, 484-491.

18. Dorozhkin, S. V. Nanosized and nanocrystalline calcium orthophosphates. *Acta Biomater.* **2010**, *6*, 715-734.

19. Núñez, N.; Sabek, J.; García-Sevillano, J.; Cantelar, E.; Escudero, A.; Ocaña, M. Solvent-controlled synthesis and luminescent properties of uniform Eu:YVO_4 nanophosphors with different morphologies. *Eur. J. Inorg. Chem.* **2013**. DOI:10.1002/ejic.201201016

20. Epple, M.; Ganesan, K.; Heumann, R.; Klesing, J.; Kovtun, A.; Neumann, S.; Sokolova, V. Application of calcium phosphate nanoparticles in biomedicine. *J. Mater. Chem.* **2010**, *20*, 18-23.

21. Dorozhkin, S. V.; Epple, M. Biological and medical significance of calcium phosphates. *Angew. Chem.-Int. Edit.* **2002**, *41*, 3130-3146.

22. Kannan, S.; Lemos, A. F.; Ferreira, J. M. F. Synthesis and mechanical performance of biological-like hydroxyapatites. *Chem. Mat.* **2006**, *18*, 2181-2186.

23. Bigi, A.; Boanini, E.; Rubini, K. Hydroxyapatite gels and nanocrystals prepared through a sol-gel process. *J. Solid State Chem.* **2004**, *177*, 3092-3098.

24. Graeve, O. A.; Kanakala, R.; Madadi, A.; Williams, B. C.; Glass, K. C. Luminescence variations in hydroxyapatites doped with Eu^{2+} and Eu^{3+} ions. *Biomaterials* **2010**, *31*, 4259-4267.

25. Lim, G. K.; Wang, J.; Ng, S. C.; Chew, C. H.; Gan, L. M. Processing of hydroxyapatite via microemulsion and emulsion routes. *Biomaterials* **1997**, *18*, 1433-1439.

26. Zhang, C. M.; Yang, J.; Quan, Z. W.; Yang, P. P.; Li, C. X.; Hou, Z. Y.; Lin, J. Hydroxyapatite Nano- and Microcrystals with Multiform Morphologies: Controllable Synthesis and Luminescence Properties. *Cryst. Growth Des.* **2009**, *9*, 2725-2733.

27. Vani, R.; Raja, S. B.; Sridevi, T. S.; Savithri, K.; Devaraj, S. N.; Girija, E. K.; Thamizhavel, A.; Kalkura, S. N. Surfactant free rapid synthesis of hydroxyapatite nanorods by a microwave irradiation method for the treatment of bone infection. *Nanotechnology* **2011**, *22*.

28. Chen, F.; Huang, P.; Zhu, Y. J.; Wu, J.; Zhang, C. L.; Cui, D. X. The photoluminescence, drug delivery and imaging properties of multifunctional Eu(3+)/Gd(3+) dual-doped hydroxyapatite nanorods. *Biomaterials* **2011**, *32*, 9031-9039.

29. Ganesan, K.; Kovtun, A.; Neumann, S.; Heumann, R.; Epple, M. Calcium phosphate nanoparticles: colloidally stabilized and made fluorescent by a phosphate-functionalized porphyrin. *J. Mater. Chem.* **2008**, *18*, 3655-3661.

30. Morgan, T. T.; Muddana, H. S.; Altinoglu, E. I.; Rouse, S. M.; Tabakovic, A.; Tabouillot, T.; Russin, T. J.; Shanmugavelandy, S. S.; Butler, P. J.; Eklund, P. C.; Yun, J. K.; Kester, M.; Adair, J. H. Encapsulation of Organic Molecules in Calcium Phosphate Nanocomposite Particles for Intracellular Imaging and Drug Delivery. *Nano Lett.* **2008**, *8*, 4108-4115.

31. Ma, M. G.; Zhu, J. F. Solvothermal Synthesis and Characterization of Hierarchically Nanostructured Hydroxyapatite Hollow Spheres. *Eur. J. Inorg. Chem.* **2009**, 5522-5526.

32. Qi, C.; Zhu, Y.-J.; Lu, B.-Q.; Zhao, X.-Y.; Zhao, J.; Chen, F. Hydroxyapatite nanosheet-assembled porous hollow microspheres: DNA-templated hydrothermal synthesis, drug delivery and protein adsorption. *J. Mater. Chem.* **2012**, *22*, 22642-22650.

33. Sokolova, V.; Prymak, O.; Meyer-Zaika, W.; Colfen, H.; Rehage, H.; Shukla, A.; Epple, M. Synthesis and characterization of DNA-functionalized calcium phosphate nanoparticles. *Materialwiss. Werkstofftech.* **2006**, *37*, 441-445.

34. Thanh, N. T. K.; Green, L. A. W. Functionalisation of nanoparticles for biomedical applications. *Nano Today* **2010**, *5*, 213-230.

35. Neumeier, M.; Hails, L. A.; Davis, S. A.; Mann, S.; Epple, M. Synthesis of fluorescent core-shell hydroxyapatite nanoparticles. *J. Mater. Chem.* **2011**, *21*, 1250-1254.

36. Mondéjar, S. P.; Kovtun, A.; Epple, M. Lanthanide-doped calcium phosphate nanoparticles with high internal crystallinity and with a shell of DNA as fluorescent probes in cell experiments. *J. Mater. Chem.* **2007**, *17*, 4153-4159.

37. Lebugle, A.; Pelle, F.; Charvillat, C.; Rousselot, I.; Chane-Ching, J. Y. Colloidal and monocrystalline Ln^{3+} doped apatite calcium phosphate as biocompatible fluorescent probes. *Chem. Commun.* **2006**, 606-608.

38. Al-Kattan, A.; Dufour, P.; Dexpert-Ghys, J.; Drouet, C. Preparation and Physicochemical Characteristics of Luminescent Apatite-Based Colloids. *J. Phys. Chem. C* **2010**, *114*, 2918-2924.

39. Klesing, J.; Chernousova, S.; Epple, M. Freeze-dried cationic calcium phosphate nanorods as versatile carriers of nucleic acids (DNA, siRNA). *J. Mater. Chem.* **2012**, *22*, 199-204.

40. Kozlova, D.; Chernousova, S.; Knuschke, T.; Buer, J.; Westendorf, A. M.; Epple, M. Cell targeting by antibody-functionalized calcium phosphate nanoparticles. *J. Mater. Chem.* **2012**, *22*, 396-404.

41. Al-Kattan, A.; Girod-Fullana, S.; Charvillat, C.; Ternet-Fontebasso, H.; Dufour, P.; Dexpert-Ghys, J.; Santran, V.; Bordère, J.; Pipy, B.; Bernad, J.; Drouet, C. Biomimetic nanocrystalline apatites: Emerging perspectives in cancer diagnosis and treatment. *Int. J. Pharm.* **2012**, *423*, 26-36.

42. Wang, Q.; Bao, Y.; Zhang, X.; Coxon, P. R.; Jayasooriya, U. A.; Chao, Y. Uptake and Toxicity Studies of Poly-Acrylic Acid Functionalized Silicon Nanoparticles in Cultured Mammalian Cells. *Adv. Healthcare Mater.* **2012**, *1*, 189-198.

43. Wang, F.; Banerjee, D.; Liu, Y. S.; Chen, X. Y.; Liu, X. G. Upconversion nanoparticles in biological labeling, imaging, and therapy. *Analyst* **2010**, *135*, 1839-1854.

44. El-Bahy, G. S.; Abdelrazek, E. M.; Allam, M. A.; Hezma, A. M. Characterization of in situ prepared nano-hydroxyapatite/polyacrylic acid (HAp/PAAc) biocomposites. *J. Appl. Polym. Sci.* **2011**, *122*, 3270-3276.

45. Bertoni, E.; Bigi, A.; Falini, G.; Panzavolta, S.; Roveri, N. Hydroxyapatite/polyacrylic acid nanocrystals. *J. Mater. Chem.* **1999**, *9*, 779-782.

46. Qu, H. B.; Wei, M. The effect of fluoride contents in fluoridated hydroxyapatite on osteoblast behavior. *Acta Biomater.* **2006**, *2*, 113-119.

47. Montazeri, N.; Jahandideh, R.; Biazar, E. Synthesis of fluorapatite-hydroxyapatite nanoparticles and toxicity investigations. *Int. J. Nanomed.* **2011**, *6*, 197-201.

48. Di, W. H.; Wang, X. J.; Chen, B. J.; Lu, S. Z.; Zhao, X. X. Effect of OH^- on the luminescent efficiency and lifetime of Tb^{3+} doped yttrium orthophosphate synthesized by solution precipitation. *J. Phys. Chem. B* **2005**, *109*, 13154-13158.

49. Zhang, C. M.; Huang, S. S.; Yang, D. M.; Kang, X. J.; Shang, M. M.; Peng, C.; Lin, J. Tunable luminescence in Ce^{3+}, Mn^{2+}-codoped calcium fluorapatite through combining emissions and modulation of excitation: a novel strategy to white light emission. *J. Mater. Chem.* **2010**, *20*, 6674-6680.

50. Porrès, L.; Holland, A.; Pålsson, L. O.; Monkman, A. P.; Kemp, C.; Beeby, A. Absolute measurements of photoluminescence quantum yields of solutions using an integrating sphere. *J. Fluoresc.* **2006**, *16*, 267-272.

51. Mosmann, T. Rapid colorimetric assay for tellular growth and survival - Application to proliferation and cyto-toxicity assays. *J. Immunol. Methods* **1983**, *65*, 55-63.

52. Klee, W. E.; Engel, G. IR spectra of phosphate ions in various apatites. *J. Inorg. Nucl. Chem.* **1970**, *32*, 1837-1843.

53. Doat, A.; Fanjul, M.; Pelle, F.; Hollande, E.; Lebugle, A. Europium-doped bioapatite: a new photostable biological probe, internalizable by human cells. *Biomaterials* **2003**, *24*, 3365-3371.

54. Kirwan, L. J.; Fawell, P. D.; van Bronswijk, W. In situ FTIR-ATR examination of poly(acrylic acid) adsorbed onto hematite at low pH. *Langmuir* **2003**, *19*, 5802-5807.

55. Dubinsky, S.; Grader, G. S.; Shter, G. E.; Silverstein, M. S. Thermal degradation of poly(acrylic acid) containing copper nitrate. *Polym. Degrad. Stabil.* **2004**, *86*, 171-178.

56. Rodríguez-Liviano, S.; Aparicio, F. J.; Rojas, T. C.; Hungria, A. B.; Chinchilla, L. E.; Ocaña, M. Microwave-Assisted Synthesis and Luminescence of Mesoporous RE Doped YPO_4 (RE = Eu, Ce, Tb, and Ce plus Tb) Nanophosphors with Lenticular Shape. *Cryst. Growth Des.* **2012**, *12*, 635-645.

57. Jean, J. H.; Ring, T. A. Processing monosized TiO_2 powders generated with HPC dispersant. *Am. Ceram. Soc. Bull.* **1986**, *65*, 1574-1577.

58. Dirksen, J. A.; Ring, T. A. Fundamentals of crystallization: Kinetic effects on particle size distributions and morphology. *Chem. Eng. Sci.* **1991**, *46*, 2389-2427.

59. Driessen, F. C. Fluoride incorporation and apatite solubility. *Caries Res.* **1973**, *7*, 297-314.

60. White, T. J.; Dong, Z. L. Structural derivation and crystal chemistry of apatites. *Acta Crystallogr. Sect. B-Struct. Sci.* **2003**, *59*, 1-16.

61. Ronda, C., *Luminescence: From Theory to Applications*. Wiley: Weinheim, 2008.

62. Höppe, H. A. Recent Developments in the Field of Inorganic Phosphors. *Angew. Chem.-Int. Edit.* **2009**, *48*, 3572-3582.

63. Martin, P.; Carlot, G.; Chevarier, A.; Den-Auwer, C.; Panczer, G. Mechanisms involved in thermal diffusion of rare earth elements in apatite. *J. Nucl. Mater.* **1999**, *275*, 268-276.

BRIEFS

Europium-doped calcium hydroxyapatite and fluoroapatite nanophosphors functionalized with poly acryl acid (PAA) have been synthesized through an one-pot microwave-assisted hydrothermal method. A novel spindle-like morphology has been obtained. The particles show a very high colloidal stability and low cytotoxicity.

SYNOPSIS